EAI Endorsed Transactions
on Energy Web

Research Article EAI.EU

Model-free predictive allocation control of large-scale pumped-storage clusters for active grid balancing via cutting-plane method

Kaiqiang Li[1], Liande Liu[1], Dongdong Zhang[1], Yang Dong[1], Ben Ao[1], Leixin Li[1], Biao Wang[1], Zhe Wang[1], Wei Zhang[1], Jingxin Yan[1], Zhong Du[1], Zhiqiang Pang[1,*]

[1] Inner Mongolia Hohhot pumped-storage power generation Co., Ltd., Hohhot, China

Abstract

INTRODUCTION: Pumped-storage hydropower plants (PSHPs) are indispensable for maintaining grid balancing amid high-penetration renewable energy integration, yet optimizing their predictive control is severely hindered by the scale of interconnected units and the resulting decision-making complexity.

OBJECTIVES: This paper aims to develop a computationally efficient and operationally scalable assignment predictive control framework tailored for modern PSHP fleets.

METHODS: To alleviate the computational burden and enhance real-time responsiveness, a model-free assignment predictive control scheme incorporating a cutting-based method is proposed to effectively streamline the solution space while guaranteeing grid stabilization.

RESULTS: Furthermore, the framework is extended to multi-PSHP clusters, establishing a cooperative model-free predictive architecture that maximizes collective balancing capacity across diverse geographical regions. Numerical simulations validate the proposed method's efficacy.

CONCLUSION: The results indicate that the proposed cooperative framework provides a practical and highly scalable solution for active grid balancing and renewable integration in large-scale PSHP systems.

Keywords: Hybrid power system, model predictive control, Lyapunov theory, optimization, cooperative control

Received on 15 December 2025, accepted on 03 May 2026, published on 12 August 2026

doi: 10.4108/ew.14126

1. Introduction

In recent years, the tremendous development of model predictive control in various domains such as, unmanned surface vehicles [1-4], multi-agent systems [5-8], formation control [9-12], energy systems [13-16], and so on, has been witnessed due to its significant realistic applications. In these domains, the control of a pumped-storage hydropower plant (PSHP) is a significant yet challenging task, which mainly focuses on the design of the control scheme of each component of the PSHP. As representative works, an MILP-based approach was presented by Chazarra et al. [17] for hourly energy and reserve scheduling of a closed-loop, variable-speed PSHP operating as a price taker., accounting for energy losses from electronic frequency converters. The model was applied to assess the PSHP's revenue under various technological conditions, showing that the integration of variable speed technology significantly increased income, with the secondary regulation reserve market being a key revenue driver. Lin et al. [18] addressed the challenge of reserve dispatchability in PSHP, which are energy-limited and subject to state-of-charge deviations that may lead to non-dispatchability. Specifically, reserve secure constraints in the day-ahead market were proposed and formulated as a distributionally robust chance-constrained approach, and their applicability was exhibited through a

*Corresponding author. Email: 979357262@qq.com

modified IEEE 118-bus system with multiple PSHPs. Furthermore, Zhang et al. [19] explored the role of variable speed and constant frequency PSHP units in stabilizing cascaded hydro-PV systems. A rule-based method was proposed to determine the optimal regulating capacity of PSHP, showing its effectiveness in mitigating real-time fluctuations of photovoltaic systems while ensuring robust performance under varying conditions. Additionally, Christe et al. [20] reported the design and practical deployment of the first direct AC/AC modular multilevel converter applied as a static frequency converter in variable-speed PSHPs, enabling efficient operation across the entire speed range, offering improved machine dynamics, reduced machine size, optimized hydraulic efficiency, and the ability to provide balance energy in pumping mode, as demonstrated by the Malta Oberstufe plant in Austria. Expanding the horizon, Tiwari et al. [21] proposed steady-state control schemes enabling variable-speed operation of PSHPs using full-scale converter-fed synchronous machines in both generating and pumping modes, ensuring seamless transitions between turbine and pump modes and demonstrating the PSHP's low-voltage ride-through capability. Along this research line, Chen et al. [22] developed a real-time, low-cost, and accurate inertia monitoring and estimation technology to address the limitations of existing methods in grids with high renewable energy penetration, which introduced a synchrophasor-based approach for detecting PSHP operations and proposed an improved inertia calculation method, integrated into a monitoring system and tested in collaboration with NERC, Dominion Energy, and Tennessee Valley Authority.

In the domain of model predictive control (MPC), some scholars have developed some interesting methods, advancing the development of control scheme. As a pioneer work, Grimm et al. [23] established robust stability results for constrained discrete-time nonlinear systems under finite-horizon MPC, without imposing specific terminal cost conditions, which introduced a definition of robustness for the MPC optimization problem and demonstrated that certain assumptions led to stability robust to small disturbances, with semiglobal or global robustness achievable under specific conditions. Han *et al.* [24] developed a nonlinear MPC framework for wastewater treatment using a self-organizing RBF neural network model and multiobjective optimization.. Subsequently, Li et al. [25] proposed a distributed model-free adaptive predictive control scheme for multiregion urban traffic networks, solved via an ADMM-based approach. In addition, Santors et al. [26] proposed a robust MPC scheme for induction motor drives by integrating indirect field-oriented control with a deadbeat-based MPC formulation, achieving robustness against parameter uncertainties. Moreover, Wu et al. [27], Lin et al. [28], Wei et al. [29], Zhao et al. [30], and Su et al. [31] offered some advanced MPC methods and theory for a variety of domains as well. However, as the system scale increases and the constraints become more intricate, traditional MPC often encounters the "curse of dimensionality," particularly when dealing with combinatorial complexity in discrete decision-making processes. To alleviate this computational burden, recent breakthroughs in deep learning have introduced promising alternatives. Specifically, Vinyals et al. [32] proposed Pointer Networks, which utilize a novel attention mechanism to handle permutation-dependent combinatorial problems, demonstrating the potential of neural architectures to learn the mapping from problem instances to optimal sequences. Building on this, Bello et al. [33] further advanced this field by integrating reinforcement learning, allowing models to search for optimal solutions in a self-supervised manner without requiring high-quality labels. Integrating these learning-based combinatorial solvers with MPC frameworks provides a new pathway for achieving real-time, high-performance control in large-scale complex systems.

However, although MPC acts as a useful tool, it is still not applied for the control of the PSHP, especially in the assignment control of the PSHP's components, due to the computational burden of solving a mixed integer programming problem. As a remedy, we employ a cutting-plane method to decrease the size of the feasible set via the proposed constraints, where a power-state-joint mixed integer optimization model is established. Then, we design a two-level recruit optimization algorithm to address the integer and real variables, respectively, which addresses the model-free assignment predictive control problem. Furthermore, we extend the single-PSHP case to the multi-PSHP system case, considering the cooperation of each PSHP, we develop a coordinated model-free assignment algorithm to achieve the multi-PSHP cooperation. In sum, the contributions of this paper are give as follows:

- Develop a cutting-plane-based model-free assignment predictive control algorithm with low computational complexity.
- Establish a cooperative model-free assignment control framework for the multi-PSHP system with coordinated terms.

The paper is organized as follows. Section II introduces the PSHP assignment formulation and the associated model assignment predictive control problem. Section III presents a cutting-plane-based solution method, which is extended to multi-PSHP systems in Section IV. Simulation results are reported in Section V, followed by concluding remarks in Section VI.

Notation: The real N-dimensional space is denoted as $\mathbb{R}^{\mathrm{N}}$, with positive real space $\mathbb{R}^{+}$, positive integer number space $\mathbb{Z}^{+}$ and $\mathrm{N} \times \mathrm{N}$ matrix space $\mathbb{R}^{\mathrm{N}\times\mathrm{N}}$. The matrix I denotes the identity matrix with compatible dimension. The operator $\otimes$ represents the Kronecker product.

2. Preliminaries and problem formulation

2.1. Description of pumped-storage hydropower plant

Define a pumped-storage hydropower plant (PSHP) with M pumping turbines. Here, these pump-turbines are all reversible, which implies that we can define an active power for j-th pumping turbine as $P_j(t)$ at the instant t for $j \in \mathcal{V}_M := \{1,2,\cdots,M\}$. For simplicity, we denote M pumping turbines in a compact form as

$$\mathbf{P}(t) = [P_1(t), P_2(t), \cdots, P_M(t)]^\top \in \mathbb{R}^M. \quad (1)$$

Note that, in realistic applications, the j-th component of the PSHP has two modes: i) power-generated and ii) pumping modes. For the power-generated mode, define the generated power of the j-th pumping turbine as

$$P_j^G(t) = \begin{cases} P_j^G(t), & P_j^G(t) > 0, \\ 0, & P_j^G(t) \le 0. \end{cases} \quad (2)$$

For the pumping mode, define the pumping power of the j-th pumping turbine as

$$P_j^P(t) = \begin{cases} -P_j^P(t), & P_j^P(t) > 0, \\ 0, & P_j^P(t) \le 0. \end{cases} \quad (3)$$

Analogously, rewriting $P_j^G(t)$ and $P_j^P(t)$ in a compact form yields

$$\mathbf{P}^G(t) = [P_1^G(t), P_2^G(t), \cdots, P_M^G(t)]^\top \in \mathbb{R}^M, \quad (4)$$

$$\mathbf{P}^P(t) = [P_1^P(t), P_2^P(t), \cdots, P_M^P(t)]^\top \in \mathbb{R}^M. \quad (5)$$

Based on the definition of $P^G(t)$ and $P^P(t)$, we give the mathmatical expression as below,

$$\mathbf{P}(t) = \mathbf{P}^G(t) - \mathbf{P}^P(t). \quad (6)$$

To represent the modes of each component of the pumping turbines, we define a mode variable as below,

$$S_j(t) = \begin{cases} 1, & \text{modei}), \\ 0, & \text{off}, \\ -1, & \text{modeii}). \end{cases} \quad (7)$$

Similar to the definition of $P_j(t)$, we denote $S_j(t)$ as below,

$$S_j(t) = S_j^G(t) - S_j^P(t) \quad (8)$$

with $S_j^G(t) \in \{0,1\}$ and $S_j^P(t) \in \{0,1\}$ being the states of the power-generated and pumping modes, respectively. Here, $S_j^G(t) = 1$ in the power-generated mode ($S_j^P(t) = 1$ in the pumping mode) denotes the j-th component of the PSHP is on, and off otherwise. Similarly, the relation of the compact forms of S_j, S_j^G, and S_j^P write

$$\mathbf{S}(t) = \mathbf{S}^G(t) - \mathbf{S}^P(t) \quad (9)$$

with $\mathbf{S}(t) = [S_1, S_2, \cdots, S_M]^\top \in \mathbb{R}^M$, $\mathbf{S}^G(t) = [S_1^G, S_2^G, \cdots, S_M^G]^\top \in \mathbb{R}^M$, and $\mathbf{S}^P(t) = [S_1^P, S_2^P, \cdots, S_M^P]^\top \in \mathbb{R}^M$.

2.2. Problem formulation

With these preliminaries, we design a performance index at the instant t as below,

$$J(t) = \alpha_1 \phi(\mathbf{P}(t)) + \alpha_2 \psi(\mathbf{S}(t), \mathbf{S}(t-1)) \quad (10)$$

with the parameters $\alpha_1 > 0$ and $\alpha_2 > 0$, where the funcitons $\phi(\cdot)$ and $\psi(\cdot)$ denote the overall operational cost at a target point and total state-switching cost of the component of the pumping turbines, respectively. Then, the power and states are necessary to fulfill the following constraints:

i) Target point power constraint: The overall power of all the components of the PSHP equals to a pre-set power P_{tar}, i.e.,

$$\sum_{j=1}^M P_j^G(t) - P_j^P(t) = P_{tar}. \quad (11)$$

ii) Secondary reserve downward amount constraint: The downward amount $\underline{R}$ of the secondary reserve is necessary to satisfy:

$$\sum_{j=1}^M P_j^G(t) - S_j^G \underline{P}_j^G \ge \underline{R} \quad (12)$$

with $\underline{P}_j^G$ being the lower bound of power of j-th component of the PSHP in the power-generated mode.

iii) Secondary reserve upward amount constraint: The upward amount $\overline{R}$ of the secondary reserve needs to fulfill:

$$\sum_{j=1}^M S_j^G \overline{P}_j^G - P_j^G(t) \ge \overline{R} \quad (13)$$

with $\overline{P}_j^G$ being the upper bound of power of j-th component of the PSHP in the power-generated mode.

iv) Power limits: The powers in power-generated and pumping modes needs to be guaranteed as below, respectively,

$$S_j^G(t) \underline{P}_i^G \le P_i^G(t) \le S_j^G(t) \overline{P}_i^G \quad (14)$$

$$S_j^P(t) \underline{P}_i^P \le P_i^G(t) \le S_j^P(t) \overline{P}_i^P, \quad (15)$$

where $\underline{P}_i^P$ and $\overline{P}_i^P$ denote the lower and upper bounds of power of j-th component of the PSHP in the pumping mode, respectively.

v) Switching Constraint: The power-generated and pumping modes do not exist at the same time, i.e.,

$$P_j^G(t) + P_j^P(t) \le 1. \tag{16}$$

With i)–iv) cases, we are ready to formulate the main model predictive control problem of the whole PSHP as below,

$$\min_{\mathbf{P},\mathbf{S}} \quad \sum_{s=t}^{H+t} J(s|t), \tag{17}$$

$$\text{s.t.} \quad \sum_{j=1}^{M} P_j^G(s|t) - P_j^P(s|t) = P_{tar} \tag{18}$$

$$\sum_{j=1}^{M} P_j^G(s|t) - S_j^G(s|t)\underline{P}_j^G \ge \underline{R} \tag{19}$$

$$\sum_{j=1}^{M} S_j^G(s|t)\overline{P}_j^G - P_j^G(s|t) \ge \overline{R} \tag{20}$$

$$S_j^G(s|t)\underline{P}_j^G \le P_j^G(s|t) \le S_j^G(s|t)\overline{P}_j^G \tag{21}$$

$$S_j^P(s|t)\underline{P}_j^P \le P_j^P(s|t) \le S_j^P(s|t)\overline{P}_j^P, \tag{22}$$

$$P_j^G(s|t) + P_j^P(s|t) \le 1. \tag{23}$$

where $*(s|t)$ denotes the s-predictive variable of the variable $*$ at the instant t.

The model predictive control optimization problem can be addressed unless the following assumption is necessary to be guaranteed.

Assumption 1: Given the feasible set

$$\Omega := \{\mathbf{S} \in \mathbb{R}^M | S_j = -1,0,1\}, \tag{24}$$

for each $\mathrm{S} \in \Omega$, $\mathrm{J}(t)$ is a convex function with respect to $\mathrm{P}(t)$.

3. Main technical results

3.1. Algorithm design

Note that, the model predictive control problem is a mixed integer optimization problem, it is time-consumed to directly solve it by branch and bound, and other approaches. So, to decrease the time complexity of solving such problem, we are ready to develop a feasible-region-cutting-based method as below.

To this end, we assume that there exists a given optimal state solutions $\mathrm{S}^*(t), \mathrm{S}^*(t+1), \cdots, \mathrm{S}^*(t+H) \in \Omega$ of $\mathrm{S}(t), \mathrm{S}(t+1), \cdots, \mathrm{S}(t+H)$. Under such given state optimal solutions, the mixed integer optimzation problem is transformed into a standard model predictive control problem, i.e.,

$$\min_{\mathbf{P}} \quad \sum_{s=t}^{H+t} J(s|t), \tag{25}$$

$$\text{s.t.} \quad \sum_{j=1}^{M} P_j^G(s|t) - P_j^P(s|t) = P_{tar} \tag{26}$$

$$\sum_{j=1}^{M} P_j^G(s|t) - S_j^{G*}(s|t)\underline{P}_j^G \ge \underline{R} \tag{27}$$

$$\sum_{j=1}^{M} S_j^{G*}(s|t)\overline{P}_j^G - P_j^G(s|t) \ge \overline{R} \tag{28}$$

$$S_j^{G*}(s|t)\underline{P}_j^G \le P_j^G(s|t) \le S_j^{G*}(s|t)\overline{P}_j^G \tag{29}$$

$$S_j^{P*}(s|t)\underline{P}_j^P \le P_j^P(s|t) \le S_j^{P*}(s|t)\overline{P}_j^P. \tag{30}$$

$$P_j^G(s|t) + P_j^P(s|t) \le 1. \tag{31}$$

Based on the above analysis, we are ready to employ the constraints as a filter, so as to cut the feasible region Ω of $\mathbf{S}$. To this end, we establish the picking principle of $\mathbf{S}$ as below,

$$\sum_{j=1}^{M} S_j^G(s|t)\underline{P}_j^G - S_j^P(s|t)\overline{P}_j^P \le P_{tar}, \tag{32}$$

$$\sum_{j=1}^{M} S_j^G(s|t)\overline{P}_j^G - S_j^P(s|t)\underline{P}_j^P \ge P_{tar}, \tag{33}$$

which consist of the cutting feasible region Ω_1. Moreover,

$$P_{tar} - \underline{R} \ge \sum_{j=1}^{M} S_j^G(s|t)\underline{P}_j^G, \tag{34}$$

$$P_{tar} + \underline{R} \ge \sum_{j=1}^{M} S_j^G(s|t)\overline{P}_j^G, \tag{35}$$

which are composed of the cutting feasible region Ω_2. Here, the relation of Ω, Ω_1, and Ω_2 is

$$\Omega_2 \subseteq \Omega_1 \subseteq \Omega, \tag{36}$$

which implies that the size of Ω_2 is smaller than the sizes of Ω and Ω_1, i.e., the complexity of constructing the optimal state $\mathbf{S}$ in Ω_2 is lower than in Ω_1 and Ω. The size of the feasible state set Ω_2 strongly depends on the reserve requirements. Larger reserve margins lead to a unique admissible commitment, whereas relaxed margins allow multiple feasible state combinations, thereby activating the proposed feasible-region-cutting-based search mechanism.

In what follows, with the assistance of these analysis, we give the following algorithm:

Step 1: Initial the size of the components of the PSHP, the target power, the forms of objective functions $\phi(\cdot)$ and $\psi(\cdot)$, the weight parameters α_1 and α_2;

Step 2: Construct the optimal state variable $\mathbf{S}(s|t)$ at the instant t for $s = t, t+1, \cdots, t+H$;

Step 3: Solve the standard model predictive control problem to obtain the optimal $\mathbf{P}^*(s|t)$ at the instant t for $s = t, t+1, \cdots, t+H$;

Step 4: With the optimal $\mathbf{P}^*(s|t)$, update the picking state $\mathbf{S}^*$ by

$$\min_{\mathbf{S}} \quad \sum_{s=t}^{H+t} J(s|t), \tag{37}$$

$$\text{s.t.} \quad P_{tar} - \underline{R} \geq \sum_{j=1}^{M} S_j^G(s|t)\underline{P}_j^G, \tag{38}$$

$$P_{tar} + \underline{R} \geq \sum_{j=1}^{M} S_j^G(s|t)\overline{P}_j^G. \tag{39}$$

$$P_j^G(s|t) + P_j^P(s|t) \leq 1. \tag{40}$$

Step 5: $t \leftarrow t+1$ and return to *Step 3* until $\|\mathbf{P}(s+1|t+1) - \mathbf{P}(s|t)\| \leq \epsilon$, where ϵ denotes a threshold, used as a stopping principle of this algorithm.

Remark 1: Note that, since the main problem is a mixed integer optimization problem, there exist both real-number and 0–1 variables, which leads to the computational complexity. Here, we employ a feasible-region-cutting strategy to decrease such complexity. In addition, we can employ a relaxation-recovery strategy to obtain an approximately optimal solution as well. Specifically, we first relax the 0–1 variables as a real variable with the range of $[0,1]$. Then, a gradient descent-based algorithm is directly applied to solve this relaxed problem. Finally, a recovery strategy is necessary to be devised to obtain the optimal solutions of the mixed integer optimization problem.

3.2. Feasibility analysis

Due to the discrete operating modes of pumped-storage units and the cumulative nature of reservoir dynamics, imposing hard water-level constraints over a finite prediction horizon may render the feasible set empty, even when the instantaneous power balance constraint is satisfied. In particular, under hard constraints, the predictive feasibility cannot be guaranteed unless the admissible water-level deviation is sufficiently large to accommodate the worst-case cumulative water-level variation. To address this issue, the water-level constraints are relaxed using a soft-constraint formulation. Specifically, slack variables are introduced to allow temporary violations of the water-level bounds, which are penalized in the objective function with a sufficiently large weight. This relaxation guarantees that the resulting quadratic program remains feasible for all admissible operating modes and prediction horizons. As a consequence, the proposed MPC scheme ensures recursive feasibility while preserving constraint satisfaction in an optimal sense. Large deviations from the reference water level are discouraged through the quadratic penalty on slack variables, whereas infeasibility caused by overly restrictive hard constraints is effectively avoided. This design choice strikes a balance between operational safety and computational tractability, which is particularly important for real-time implementation in large-scale PSHP.

3.3. Multi-PSHP cooperation

Based on the main technical results, we are ready to give some corollaries with respect to multi-PSHP cooperation as below. First, it is necessary to define a multi-PSHP system. Define a node set $\mathcal{V}_N := \{1,2,\cdots,N\}$, an edge set $\mathcal{E} := \{(i,i')|i,i' \in \mathcal{V}_N\} \subseteq \mathcal{V}_N \times \mathcal{V}_N$, and an adjacent matrix $\mathcal{A} \in \mathbb{R}^{N\times N}$. Here, the cooperation of each PSHP is achieved by the communication among PSHPs, and thus self-loop does not exist in this study. Define the degree of $d_i = \sum_{i'=1}^{N} a_{i,j}$, inducing a degree matrix $\mathcal{D} = \text{diag}\{d_1, d_2, \cdots, d_N\}$. Define the Laplacian matrix $\mathcal{L} = \mathcal{D} - \mathcal{A}$., which immediately leads to the following assumption.

Assumption 2: The network induced by the tuple $(\mathcal{V}, \mathcal{E}, \mathcal{A})$ is connected if the network is undirected. If the network is directed, then it is strongly conected.

Note that, Assumption 2 does not require that this network is balanced.

Now, one can establish the multi-PSHP coordinated model predictive control problem as below,

$$\min_{\mathbf{P}_i, \mathbf{S}_i} \quad \sum_{i=1}^{N} \sum_{s=t}^{H+t} J_i(s|t), \tag{41}$$

$$\text{s.t.} \quad \sum_{j=1}^{M} P_{i,j}^G(s|t) - P_{i,j}^P(s|t) = P_{i,tar} \tag{42}$$

$$\sum_{j=1}^{M} P_{i,j}^G(s|t) - S_{i,j}^G(s|t)\underline{P}_{i,j}^G \geq \underline{R}_i \tag{43}$$

$$\sum_{j=1}^{M} S_{i,j}^G(s|t)\overline{P}_{i,j}^G - P_{i,j}^G(s|t) \geq \overline{R}_i \tag{44}$$

$$S_{i,j}^G(s|t)\underline{P}_{i,j}^G \leq P_{i,j}^G(s|t) \leq S_{i,j}^G(s|t)\overline{P}_{i,j}^G \tag{45}$$

$$S_{i,j}^P(s|t)\underline{P}_{i,j}^P \leq P_{i,j}^P(s|t) \leq S_{i,j}^P(s|t)\overline{P}_{i,j}^P, \tag{46}$$

$$P_{i,j}^G(s|t) + P_{i,j}^P(s|t) \leq 1. \tag{47}$$

$$\xi_1(\mathbf{P}_1, \mathbf{P}_2, \cdots, \mathbf{P}_N) = 0, \tag{48}$$

$$\xi_2(\mathbf{P}_1, \mathbf{P}_2, \cdots, \mathbf{P}_N) \leq 0, \tag{49}$$

with $\mathbf{P}_i$ and $\mathbf{S}_i$ being the power and state of the i-th PSHP, respectively, where J_i denotes the performance index of PSHP i, and the functions $\xi_1(\cdot)$ and $\xi_2(\cdot)$ act as the role of the equality-form and inequality-form cooperative terms, respectively.

To guarantee the distributed manner of the solving process of the multi-PSHP coordinated model predictive control problem, we now design a distributed state estimator as below,

$$\dot{\hat{x}}_{i,i'} = \sum_{i''=1}^{N} a_{i',i''}\left(\hat{x}_{i'',i'} - \hat{x}_{i,i'}\right) + a_{i,i'}\left(x_{i'} - \hat{x}_{i,i''}\right), \tag{50}$$

where the symbol x denotes the state of the multi-PSHP system, and $\hat{x}_{i,i'}$ denotes the state estimation of i-th PSHP with respect to i'-th PSHP. Here, the variable x represents the power $\mathbf{P}$. Therefore, the multi-PSHP coordinated model predictive control problem is tranformed into N model predictive control sub-problems, only depending on itself state and the state estimations with respect to other PSHPs. The concrete mathmatical form of the i-th sub-problem is given as below,

$$\min_{\mathbf{P}_i,\mathbf{S}_i} \quad \sum_{s=t}^{H+t} J_i\,(s|t), \tag{51}$$

$$\text{s.t.} \quad \sum_{j=1}^{M} P_{i,j}^{G}\,(s|t) - P_{i,j}^{P}(s|t) = P_{i,tar} \tag{52}$$

$$\sum_{j=1}^{M} P_{i,j}^{G}\,(s|t) - S_{i,j}^{G}(s|t)\underline{P}_{i,j}^{G} \geq \underline{R}_i \tag{53}$$

$$\sum_{j=1}^{M} S_{i,j}^{G}\,(s|t)\overline{P}_{i,j}^{G} - P_{i,j}^{G}(s|t) \geq \overline{R}_i \tag{54}$$

$$S_{i,j}^{G}(s|t)\underline{P}_{i,j}^{G} \leq P_{i,j}^{G}(s|t) \leq S_{i,j}^{G}(s|t)\overline{P}_{i,j}^{G} \tag{55}$$

$$S_{i,j}^{P}(s|t)\underline{P}_{i,j}^{P} \leq P_{i,j}^{P}(s|t) \leq S_{i,j}^{P}(s|t)\overline{P}_{i,j}^{P}, \tag{56}$$

$$\xi_1(\widehat{\mathbf{P}}_1, \widehat{\mathbf{P}}_2, \cdots, \widehat{\mathbf{P}}_i, \cdots, \widehat{\mathbf{P}}_N) = 0, \tag{57}$$

$$\xi_2(\widehat{\mathbf{P}}_1, \widehat{\mathbf{P}}_2, \cdots, \widehat{\mathbf{P}}_i, \cdots, \widehat{\mathbf{P}}_N) \leq 0. \tag{58}$$

For the model predictive control sub-problem governed by the multi-PSHP system, we are ready to develop a distributed algorithm to address it.

Step 1: Initial the size of the multi-PSHP system, the adjacent matrix, the size of the components of each PSHP, the target power, the forms of objective functions $\phi_i(\cdot)$ and $\psi_i(\cdot)$, the weight parameters $\alpha_{i,1}$ and $\alpha_{i,2}$ of the i-th PSHP;

Step 2: Construct the communication backbone by the pre-set adjacent matrix;

Step 3: For i-th PSHP, construct the optimal state variable $\mathbf{S}_i(s|t)$ at the instant t for $s = t, t+1, \cdots, t+H$;

Step 4: For i-th PSHP, solve the model predictive control sub-problem to obtain the optimal $\mathbf{P}_i^*(s|t)$ at the instant t for $s = t, t+1, \cdots, t+H$;

Step 5: For i-th PSHP, with the optimal $\mathbf{P}_i^*(s|t)$, update the picking state $\mathbf{S}_i^*$ by

$$\min_{\mathbf{S}_i} \quad \sum_{s=t}^{H+t} J\,(s|t), \tag{59}$$

$$\text{s.t.} \quad P_{i,tar} - \underline{R} \geq \sum_{j=1}^{M} S_{i,j}^{G}\,(s|t)\underline{P}_{i,j}^{G}, \tag{60}$$

$$P_{i,tar} + \underline{R} \geq \sum_{j=1}^{M} S_{i,j}^{G}\,(s|t)\overline{P}_{i,j}^{G}. \tag{61}$$

Step 6: Estimate the states of other PSHPs by the developed distributed state estimator with the assistance of the constructed communication backbone;

Step 7: $t \leftarrow t+1$ and return to *Step 3* until $\|\mathbf{P}_i(s+1|t+1) - \mathbf{P}_i(s|t)\| \leq \epsilon$, where ϵ denotes a threshold, used as a stopping principle of this algorithm.

Theorem 1: For the multi-PSHP system governed by M components and the distributed state estimator, one has that

$$\lim_{t\to\infty} \hat{x}_{i,i'} = x_{i'}. \tag{62}$$

Proof: For simplicity, we define

$$\mathbf{x} := [x_1^\top, x_2^\top, \cdots, x_N^\top]^\top \tag{63}$$

and

$$\hat{\mathbf{x}} = [\hat{x}_{1,1}^\top, \hat{x}_{2,1}^\top, \cdots, \hat{x}_{1,2}^\top, \cdots, \hat{x}_{N,N}^\top]^\top. \tag{64}$$

So, we rewrite the distributed state estimator in a compact form as below,

$$\dot{\hat{\mathbf{x}}} = \Phi\hat{\mathbf{x}} + g(\mathbf{x}) \tag{65}$$

with the system state matrix

$$\Phi = -(I \otimes \mathcal{L} + \mathcal{B}), \tag{66}$$

the matrix

$$\mathcal{B} = \mathrm{diag}\{a_{i,i'}\}, i, i' \in \mathcal{V}, \tag{67}$$

and the function

$$g(\mathbf{x}) = [a_{1,1}x_1^\top, \cdots, a_{N,1}x_1^\top, a_{1,2}x_2^\top, \cdots, a_{N,N}x_N^\top]^\top. \tag{68}$$

Note that, since the matrix $\mathcal{B}$ has N elements locating in the diagonal posiitons, which implies that $\mathcal{B}$ is positive definite and thus all the eigenvalues of $\mathcal{B}$ is positive. Moreover, the Laplacian matrix $\mathcal{L}$ is positive semi-definite, which implies that there exists at least an 0 eignevalue. Therefore, $I \otimes \mathcal{L} + \mathcal{B}$ is of positive definiteness, and thereby Φ is Hurwitz, which immediately leads to

$$\lim_{t\to\infty} \dot{\hat{\mathbf{x}}}(t) = 0 \tag{69}$$

and hence

$$\lim_{t\to\infty} \hat{x}_{i,i'}(t) = x_{i'}, i, i' \in \mathcal{V}. \tag{70}$$

The proof is thus completed.

3.4. Numerical simulations

First, according to Assumption 1, we pick the objective functions ϕ and ψ as below,

$$\phi(\mathbf{P}(s|t)) = \sum_{j=1}^{M} \left(P_j^G(s|t)\right)^2 + \sum_{j=1}^{M} \left(P_j^P(s|t)\right)^2.$$

$$\psi(\mathbf{S}(s|t), \mathbf{S}(s-1|t)) = \sum_{j=1}^{M} (c_j^{\text{on}} [S_j^G(s|t) - S_j^G(s-1|t)]_+$$

$$+ c_j^{\text{off}} [S_j^G(s-1|t) - S_j^G(s|t)]_+)$$

$$+ \sum_{j=1}^{M} (c_j^{\text{onP}} [S_j^P(s|t) - S_j^P(s-1|t)]_+ + c_j^{\text{offP}} [S_j^P(s-1|t) - S_j^P(s|t)]_+), \quad (71)$$

where the operator $[\cdot]_+ \triangleq \max\{\cdot, 0\}$ extracts the positive part of its argument, c_j^{on} and c_j^{off} denote the start-up and shut-down costs associated with switching the generating mode of unit j, respectively, while c_j^{onP} and c_j^{offP} represent the corresponding switching costs for the pumping mode. Here, the terms $[S_j^G(s|t) - S_j^G(s-1|t)]_+$ and $[S_j^G(s-1|t) - S_j^G(s|t)]_+$ capture the on–off transitions of the generating mode, and the pumping-mode transitions are defined in an analogous manner.

3.5. Static power assignment

Case i)

In this case, a pumped-storage hydropower system consisting of $\mathrm{M} = 5$ identical units is considered. The prediction horizon of the proposed MPC framework is set to $\mathrm{H} = 1$, which provides a reasonable trade-off between computational complexity and control performance. The control objective is to track a prescribed target power $\mathrm{P_{tar}} = 160$, while allowing a limited regulation margin characterized by $\mathrm{R_{down}} = 20$ and $\mathrm{R_{up}} = 20$ to accommodate feasible unit commitment and power allocation. For each pumped-storage unit, the minimum and maximum power outputs in the generating mode are specified as $\underline{\mathrm{P}}^{\mathrm{G}} = 20$ and $\overline{\mathrm{P}}^{\mathrm{G}} = 80$, respectively, whereas the corresponding power limits in the pumping mode are given by $\underline{\mathrm{P}}^{\mathrm{P}} = 20$ and $\overline{\mathrm{P}}^{\mathrm{P}} = 80$.

The weighting parameters in the objective function are chosen as $\alpha_1 = 1.0$ and $\alpha_2 = 10.0$, where α_1 penalizes the continuous operating cost associated with power regulation, and α_2 imposes a relatively stronger penalty on the discrete switching cost so as to discourage frequent transitions between operating modes. The start-up and shut-down costs for the generating mode are uniformly set to $\mathrm{c_j^{on}} = \mathrm{c_j^{off}} = 10$, while those for the pumping mode are selected as $\mathrm{c_j^{onP}} = \mathrm{c_j^{offP}} = 8$, reflecting the asymmetric operational characteristics of the two modes. Finally, the convergence tolerance of the iterative MPC procedure is fixed at $\varepsilon_{\mathrm{conv}} = 10^{-3}$, which ensures numerical stability while avoiding unnecessary iterations. The executing performance of the PSHP under Case i) is shown in Fig. 1.

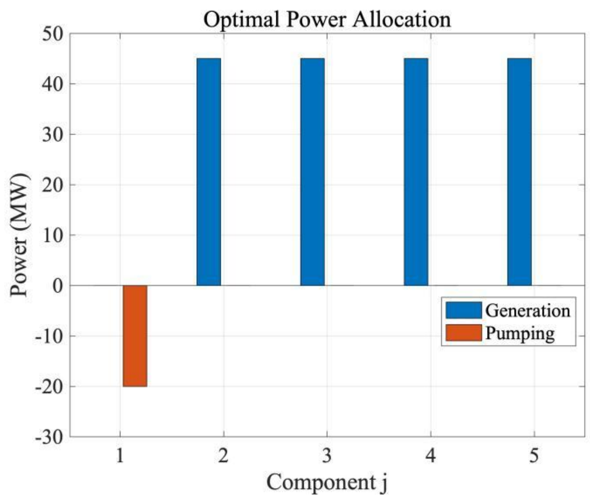

Figure 1. The performance of the power and states of the components of the PSHP under Case i)

Case ii)

To further examine the behavior of the proposed control scheme under a different operating configuration, a pumped-storage hydropower plant composed of $\mathrm{M} = 7$ units is considered. In this case, the prediction horizon is intentionally shortened to $\mathrm{H} = 1$ in order to highlight the instantaneous decision-making property of the controller and to facilitate the observation of convergence characteristics. The system is required to deliver a target power of $\mathrm{P_{tar}} = 130$, while satisfying asymmetric secondary reserve requirements, namely a downward reserve margin of $\mathrm{R_{down}} = 10$ and an upward reserve margin of $\mathrm{R_{up}} = 15$.

Each unit is subject to identical operating limits in both generating and pumping modes. Specifically, the admissible power range in the generating mode is defined by $\underline{\mathrm{P}}^{\mathrm{G}} = 10$ and $\overline{\mathrm{P}}^{\mathrm{G}} = 90$, whereas the pumping mode is constrained by $\underline{\mathrm{P}}^{\mathrm{P}} = 10$ and $\overline{\mathrm{P}}^{\mathrm{P}} = 90$. Compared with the previous setup, greater emphasis is placed on power regulation performance by selecting the weighting parameter $\alpha_1 = 10.0$, while the switching penalty weight is reduced to $\alpha_2 = 1.0$, thereby allowing more flexibility in mode transitions when beneficial for tracking the target power.

The mode transition costs are specified to reflect moderate asymmetry between activation and deactivation processes. In particular, the on/off costs associated with the generating mode are chosen as $\mathrm{c_j^{on}} = 10$ and $\mathrm{c_j^{off}} = 8$, respectively, while the corresponding costs in the pumping mode are set to $\mathrm{c_j^{onP}} = 10$ and $\mathrm{c_j^{offP}} = 8$ for all units $\mathrm{j} \in \mathcal{V}_{\mathrm{M}}$. The executing performance of the PSHP under Case i) is shown in Fig. 2.

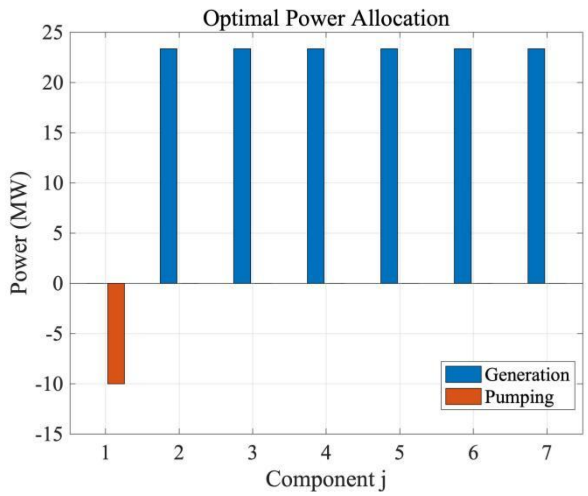

Figure 2. The performance of the power and states of the components of the PSHP under Case ii)

Case iii)

In this scenario, the control configuration is characterized by relatively tight operating margins and a balanced treatment of continuous and discrete decision variables. The target power is specified as $P_{tar} = 110$, together with a downward reserve requirement of $R_{down} = 12$ and an upward reserve requirement of $R_{up} = 10$, which collectively impose a more restrictive feasible operating region compared with the previous cases. The plant consists of $M = 9$ pumped-storage units, each of which is constrained to operate within a narrow power range in both generating and pumping modes, i.e., $\underline{P}^G = \underline{P}^P = 20$ and $\overline{P}^G = \overline{P}^P = 50$.

The prediction horizon is fixed at $H = 1$, emphasizing instantaneous regulation decisions and enabling a clear assessment of the steady-state behavior of the proposed MPC scheme. Equal weighting is assigned to the power regulation cost and the switching cost by selecting $\alpha_1 = \alpha_2 = 1.0$, which reflects a balanced control objective without explicitly prioritizing either smooth power allocation or mode persistence. Furthermore, asymmetric switching penalties are introduced, with lower activation costs ($c_j^{on} = c_j^{onP} = 8$) and higher deactivation costs ($c_j^{off} = c_j^{offP} = 10$), thereby discouraging unnecessary shutdowns once a unit is committed. The executing performance of the PSHP under Case i) is shown in Fig. 3.

Comparison analysis

A comparative analysis of the three simulation cases reveals distinct control behaviors induced by different parameter configurations. In Case 1, a relatively long prediction horizon and a dominant switching penalty encourage mode persistence and smooth operational trajectories, resulting in limited state transitions and gradual power redistribution among units. This setup is particularly suitable for applications where frequent start-up and shut-down actions are undesirable due to mechanical wear or operational constraints.

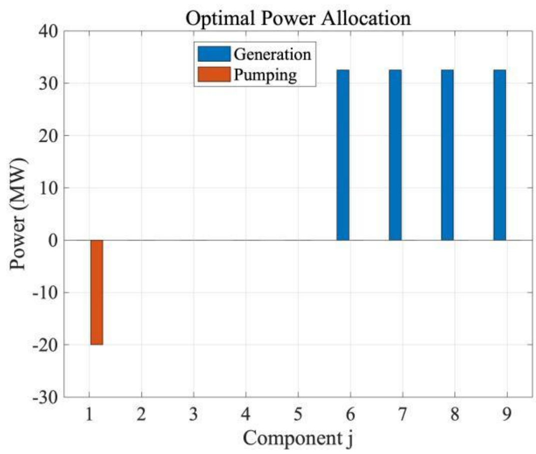

Figure 3. The performance of the power and states of the components of the PSHP under Case iii)

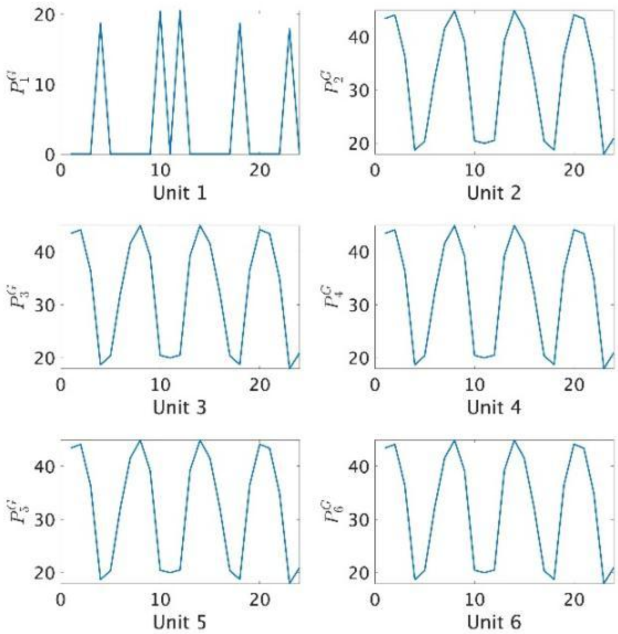

Figure 4. The dynamic performance of the power P_j^G of the components of the PSHP under a time-variant signal $P_{tar}(t)$

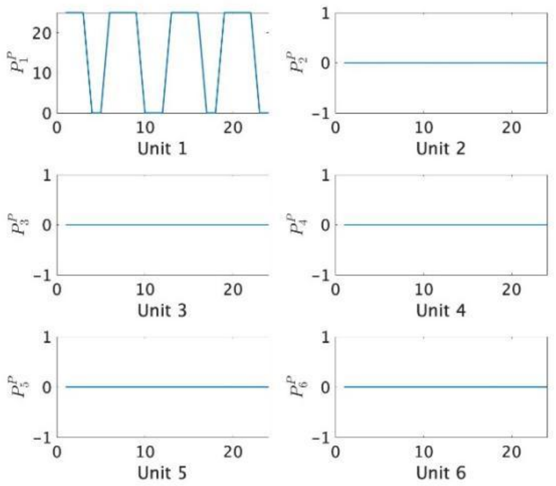

Figure 5. The dynamic performance of the power P_j^P of the components of the PSHP under a time-variant signal $P_{tar}(t)$

In contrast, Case 2 adopts a myopic prediction horizon and places greater emphasis on power regulation accuracy by assigning a larger weight to the continuous cost term. As a consequence, the controller exhibits increased flexibility in adjusting unit commitment and power outputs, leading to more frequent mode transitions but improved tracking performance with respect to the target power. This case highlights the capability of the proposed framework to accommodate fast regulation requirements.

Case 3 represents a more constrained operating environment, featuring a larger number of units with narrower admissible power ranges and balanced cost weights. Under this configuration, the controller must simultaneously satisfy tight reserve constraints and manage switching decisions without a clear priority between continuous and discrete objectives. The resulting behavior demonstrates the robustness of the proposed MPC scheme in handling dense feasible regions and competing performance criteria, thereby validating its applicability to practical large-scale pumped-storage systems.

3.6. Dynamic power assignment

To evaluate the performance of the proposed MPC framework under time-varying operating conditions, a dynamic dispatch scenario is considered. The pumped-storage hydropower plant consists of $M = 6$ units, and the prediction horizon is fixed at $H = 1$ to emphasize real-time responsiveness rather than long-term anticipation. The target power reference is no longer constant, but instead follows a periodic trajectory over a 24-hour horizon, defined as

$$P_{tar}(t) = 50\sin(t) + 150, \quad t = 1,2,\dots,24,(72)$$

which mimics typical daily load fluctuations encountered in power system operations. This time-varying reference introduces additional challenges to the controller, as both power allocation and unit commitment decisions must continuously adapt to changing demand levels.

To ensure sufficient flexibility for regulation, the downward and upward reserve requirements are set to $R_{down} = 15$ and $R_{up} = 12$, respectively. Each unit operates under asymmetric power limits in different modes: in the generating mode, the admissible power range is specified by $\underline{P}^G = 15$ and $\overline{P}^G = 65$, while in the pumping mode the limits are given by $\underline{P}^P = 25$ and $\overline{P}^P = 45$. Such asymmetric bounds reflect practical differences between generation and pumping efficiencies and further increase the complexity of the control problem.

The objective function weights are chosen as $\alpha_1 = 2.0$ and $\alpha_2 = 1.0$, indicating a moderate emphasis on tracking the time-varying power reference while still accounting for the cost associated with mode transitions. Moreover, asymmetric switching penalties are introduced to capture distinct operational preferences: lower costs are assigned to activating the generating mode ($c_j^{on} = 8$) and deactivating the pumping mode ($c_j^{offP} = 8$), whereas higher penalties are imposed on shutting down generation ($c_j^{off} = 12$) and starting pumping ($c_j^{onP} = 12$). This configuration implicitly favors generation persistence during high-demand periods and discourages unnecessary transitions into the pumping mode when rapid power support is required.

Finally, the convergence tolerance is set to $\varepsilon_{conv} = 10^{-3}$, and the maximum number of MPC iterations is aligned with the length of the scheduling horizon, i.e., $\mathrm{maxIter} = 24$, ensuring that the controller updates its decisions consistently over the entire daily operating cycle.

The performances of the power in power-generated and pumping modes are shown in Figs. 4 and 5. It is observed from Figs. 4 and 5 that components (Units) 2–6 are always on the power-generated mode, whereas component 1 varies as the target power P_{tar}, i.e., component 1 switches in the power-generated and pumping modes.

4. Conclusion

To address the assignment control issue of the PSHP, we establish a model-free assignment predictive control framework, where a cutting-plane method is employed to decrease the computational burden. Additionally, a cooperative assignment predictive control framework of the multi-PSHP system with the coordinated terms is constrcuted. Future work will focus on the Lyapunov-based model predictive control of the PSHP with a realistic model.

References

[1] Jiang L, Wang C, Shang X, Zhang Z. Two-step event-triggered data driven model predictive control for trajectory tracking of unmanned surface vessel under environmental disturbances. IEEE Trans Autom Sci Eng. 2025;22:16801-13.

[2] Zheng H, Li J, Tian Z, Liu C, Wu W. Hybrid physics-learning model based predictive control for trajectory tracking of unmanned surface vehicles. IEEE Trans Intell Transp Syst. 2024;25(9):11522-33.

[3] Lyu G, Peng Z, Wang J. Safety-certified parallel model predictive control of autonomous surface vehicles via neurodynamic optimization. IEEE/CAA J Autom Sin. 2025;12(10):2056-66.

[4] Jia Z, Lu H, Chen H, Zhang W. Robust distributed cooperative rendezvous control for heterogeneous marine vehicles using model predictive control. IEEE Trans Veh Technol. 2024;73(8):11002-13.

[5] Li H, Li X. Distributed fixed-time consensus of discrete-time heterogeneous multi-agent systems via predictive mechanism and Lyapunov approach. IEEE Trans Circuits Syst II. 2024;71(1):321-5.

[6] Li H, Li X. Finite-time predictive consensus for discrete-time heterogeneous multi-agent systems over switching digraphs. IEEE Trans Circuits Syst II. 2023;70(6):2136-40.

[7] Huang Y, Liu G-P, Yu Y, Hu W. Data-driven distributed predictive tracking control for heterogeneous nonlinear multiagent systems with communication delays. IEEE Trans Autom Control. 2024;69(7):4786-92.

[8] Luo W, Lu P, Du C, Liu H. Cooperative output tracking control of heterogeneous multi-agent systems with random communication constraints: an observer-based predictive control approach. IEEE Trans Circuits Syst II. 2022;69(3):1139-43.

[9] Huang D, Li H, Li X. Formation of generic uavs-usvs system under distributed model predictive control scheme. IEEE Trans Circuits Syst II. 2020;67(12):3123-7.

[10] Sun Z, Wu B, Wang D, Chen J. Event-triggered model predictive control of spacecraft formation. IEEE Trans Autom Sci Eng. 2025;22:7696-7711.

[11] Chen Q, Jin Y, Wang T, Wang Y, Yan T, Long Y. UAV formation control under communication constraints based on distributed model predictive control. IEEE Access. 2022;10:126494-507.

[12] Wang Z, Diao W, Li W, Xu B. Formation tracking control of auvs subject to disturbances via distributed adaptive sliding model predictive control. IEEE Trans Veh Technol. 2025;74(7):10067-80.

[13] Vašak M, Banjac A, Hure N, Novak H, Marušić D, Lešić V. Modular hierarchical model predictive control for coordinated and holistic energy management of buildings. IEEE Trans Energy Convers. 2021;36(4):2670-82.

[14] Agharazi H, Prica M, Mondal A, Fu Q, Bhavaraju V, May RD, Fok K, Dise S, Swierc A, Loparo KA. Installation and testing of a two-level model predictive control building energy management system. IEEE Trans Control Syst Technol. 2024;32(2):326-39.

[15] Song D, Chang Q, Zheng S, Yang S, Yang J, Joo YH. Adaptive model predictive control for yaw system of variable-speed wind turbines. J Mod Power Syst Clean Energy. 2021;9(1):219-24.

[16] Liu X, Suo Y, Zhang Z, Song X, Zhou J. A new model predictive current control strategy for hybrid energy storage system considering the soc of the supercapacitor. IEEE J Emerg Sel Top Power Electron. 2023;11(1):325-38.

[17] Chazarra M, Pérez-Díaz JI, García-González J. Optimal joint energy and secondary regulation reserve hourly scheduling of variable speed pumped storage hydropower plants. IEEE Trans Power Syst. 2018;33(1):103-15.

[18] Liu Y, Wu L, Yang Y, Chen Y, Baldick R, Bo R. Secured reserve scheduling of pumped-storage hydropower plants in iso day-ahead market. IEEE Trans Power Syst. 2021;36(6):5722-33.

[19] Zhang S, Xiang Y, Liu J, Liu J, Yang J, Zhao X, Jawad S, Wang J. A regulating capacity determination method for pumped storage hydropower to restrain pv generation fluctuations. CSEE J Power Energy Syst. 2022;8(1):304-16.

[20] Christe A, Faulstich A, Vasiladiotis M, Steinmann P. World's first fully rated direct ac/ac mmc for variable-speed pumped-storage hydropower plants. IEEE Trans Ind Electron. 2023;70(7):6898-907.

[21] Tiwari R, Nilsen R, Mo O, Nysveen A. Control methods for operation of pumped storage plants with full-size back-to-back converter fed synchronous machines. IEEE Trans Ind Appl. 2023;59(6):6792-803.

[22] Chen C, Li H, Baldwin MW, Wen Y, Zeng C, Zhu L, Qiu W, Liu Y. Online inertia estimation: a pumped storage hydropower turn-off traces based-method in large interconnection systems. IEEE Trans Ind Inform. 2025;21(12):9712-23.

[23] Grimm G, Messina MJ, Tuna SE, Teel AR. Nominally robust model predictive control with state constraints. IEEE Trans Autom Control. 2007;52(10):1856-70.

[24] Han H, Qiao J. Nonlinear model-predictive control for industrial processes: an application to wastewater treatment process. IEEE Trans Ind Electron. 2014;61(4):1970-82.

[25] Li D, De Schutter B. Distributed model-free adaptive predictive control for urban traffic networks. IEEE Trans Control Syst Technol. 2022;30(1):180-92.

[26] Santos TB, Oliani I, Figueiredo R, Albieiro D, Pelizari A, Sguarezi Filho AJ. Robust finite control set model predictive current control for induction motor using deadbeat approach in stationary frame. IEEE Access. 2023;11:13067-78.

[27] Wu W, Qiu L, Rodriguez J, Liu X, Ma J, Fang Y. Data-driven finite control-set model predictive control for modular multilevel converter. IEEE J Emerg Sel Top Power Electron. 2023;11(1):523-31.

[28] Lin X, Liu J, Liu Z, Gao Y, Peretti L, Wu L. Model-free current predictive control for pmsms with ultralocal model employing fixed-time observer and extremum-seeking method. IEEE Trans Power Electron. 2025;40(8):10682-93.

[29] Wei Y, Young H, Ke D, Wang F, Qi H, Rodríguez J. Model-free predictive control using sinusoidal generalized universal model for pmsm drives. IEEE Trans Ind Electron. 2024;71(11):13720-31.

[30] Zhao P, Ma J, Liu X, Qiu L, Liu C, Zhang Z, Fang Y. An online neural network approximator-based model-free predictive control approach for power converters. IEEE Trans Power Electron. 2025;40(10):15757-67.

[31] Su J, Wang H, Li P, Yang G. Dimension-reduced direct speed control based on line-constrained explicit model predictive control for ipmsm. IEEE Trans Ind Electron. 2025;72(12):14963-8.

[32] Vinyals O, Fortunato M, Jaitly N. Pointer networks. Advances in neural information processing systems, 2015, 28.

[33] Bello I, Pham H, Le Q V, et al. Neural combinatorial optimization with reinforcement learning. arXiv preprint arXiv:1611.09940, 2016.